COMPDYN 2015
5th ECCOMAS Thematic Conference on
Computational Methods in Structural Dynamics and Earthquake Engineering
M. Papadrakakis, V. Papadopoulos, V. Plevris (eds.)
Crete Island, Greece, 25–27 May 2015

A PERFECTLY MATCHED LAYER FOR SEISMIC WAVE PROPAGATION IN UNBOUNDED DOMAIN BY USING HETEROGENEOUS MULTI-TIME STEP SUBDOMAIN METHODS

Zafati E.[1], Brun M.[1], and Djeran-Maigre I.[1]

[1]INSA de Lyon
Batiment Coulomb 20, Avenue A. Einstein 69621 Villeurbanne cedex (France)
e-mail: eliass.zafati@insa-lyon.fr

Keywords: wave propagation, perfectly matched layers, multi−step coupling algorithms.

Abstract. *In the framework of the Finite Element Method, Perfectly Matched Layer (or PML) is recognized as a very effective tool for reproducing unbounded domains (Basu et al. [13]). Nonetheless, the computation time required by the PML may be large, especially when an explicit time integration scheme is adopted for dealing with the wave propagation problem both in the domain of interest and in the PML medium (Basu et al. [13]). The paper proposed to investigate subdomain strategies enabling to choose the appropriate time integration scheme in the PML with its own time step, independently on the choice of the explicit time scheme in the domain of interest associated with a fine time step satisfying the stability criterion (CFL condition). The investigated subdomain strategy, proposed by Gravouil and Combescure [14], is based on the Schur dual approach, characterized by the introduction of Lagrange multipliers at the interface between subdomains for ensuring the velocity continuity.*

1 Introduction

The simulation of wave motion in unbounded media often compels a numerical solution using artificial boundaries surrounding the finite computational domain. Several techniques have been developped to repoduce unbounded domain: the infinite elements (Bettess [1]), the absorbing boundaries methods (Enquist $et\ al.$ [2]) and the absorbing layers methods such as the Rayleigh damping layers (Semblat $et\ al.$ [3], Rajagopal $et\ al.$ [4] et Zafati $et\ al.$ [5]) and the perfectly matched layers (PML) (Chew $et\ al.$ [6]).

The perfectly matched layers (PML) is an absorbing layer method which surrounds the computational domain with an uniform thickness layer. The PMLs are characterized by their capabilities of providing the same attenuation for all frequencies without, from the analytical point of view, reflections at the interface for all angles of incidence and frequencies.

In the beginning, the PMLs have been developed for the Maxwell's equations by Bérenger $et\ al.$ [7] using a field-splitting formulation and have became one of the most widely used methods in the simulation of wave propagation problems in unbounded media. The technique was then adapted to the elastodynamics equations. Hastings $et\ al.$ [8] extended the PML from electromagnetics to elastodynamics using a formulation in terms of displacement potentials implemented in the finite difference framework. Using also the finite difference method, Chew $et\ al.$ [6] introduced a new split-field formulation, velocity$-$stress, applied to the isotropic medium and also implemented using the finite difference method. Later on, Collino $et\ al.$ [9] proposed a finite difference split$-$field formulation similar to Chew $et\ al.$ [6], applied to anisotropic media. In [10], Wang *et al.* developed a new PML formulation, called C$-$PML, using the convolution features adapted to the finite difference method. Matzen [11] extended the C-PML approach to the finite element method. In this work, we are interested in an unsplit$-$field formulation developed for the finite element method in [12] and [13] by Basu $et\ al.$ for applications involving 2D media.

When addressing the numerical implementation, it is often interesting, for several applications, to use an implicit time integration scheme (the average acceleration method) for the absorbing layer such as the PML, while the physical domain is integrated in time by an explicit scheme (central difference method). The subdomain method proposed by Gravouil and Combescure [14] provides the suitable properties for coupling an explicit integrator for the subdomain of interest with an implicit one for the absorbing layers. The method follows a dual Schur approach by ensuring the velocity continuity at the interface through Lagrange multipliers. The method is proved to be stable for any Newmark integrators [15] using the so-called energy method (Hughes, [16]). It leads to the first order of accuracy when coupling second order accurate time integration schemes due to a slight spurious dissipation at the interface as soon as different time steps are adopted. When adopting the same time step, second order of accuracy is achieved [17].

In this paper, the technique of the absorbing layers using the PMLs is adopted. First, we propose to present the multi$-$time step coupling algorithm between the PML, formulated by Basu $et\ al.$ in [13], and the physical domain assumed to be linear isotropic medium. Then, we report numerical results using 2D applications and demonstrating the efficiency of the coupling method.

2 Perfectly matched layer

2.1 Strong form of the PML in frequency domain

The PML model used in this work has been developed by Basu *et al* ([13] and [18]). It is built using the classical elastodynamic equations by introducing the complex transform functions λ_i. The main idea is to replace the real coordinates x_i with the complex ones $x_i \rightarrow \tilde{x}_i : \mathbb{R} \rightarrow \mathbb{C}$. The complex coordinates are defined as:

$$\frac{\partial \tilde{x}_i}{\partial x_i} = \lambda_i(x_i) = 1 + f_i^e(x_i) - i\frac{f_i^p(x_i)}{k_s} \tag{1}$$

where $k_s = \frac{\omega}{c_s}$ (c_s being the S-wave velocity) and f_i^e, f_i^p are positive functions that vanish at the interfaces between the PML and the physical domain. The function f_i^p is introduced to attenuate the propagative waves in the x_i direction, whereas the function f_i^e attenuates the evanescent wave. The dependence on the angular frequency of the complex term in Eq. (1), in the equation (1), makes the imaginary part of the wave number independent of the frequency. In other words, all frequencies are damped in the same way.

The PML formulation is obtained by modifying the governing equations defined in the frequency domain. The equations are re-written by substituting x_i by $\tilde{x}_i$ as follows:

$$\begin{aligned} \Sigma_j \frac{1}{\lambda_j(x_j)} \frac{\partial \sigma_{ij}}{\partial x_j} &= -\omega^2 \rho u_j \\ \sigma_{ij} &= \Sigma_{k,l} C_{ijkl} \varepsilon_{ij} \\ \varepsilon_{ij} &= \frac{1}{2}\left[\frac{1}{\lambda_j(x_j)}\frac{\partial u_i}{\partial x_j} + \frac{1}{\lambda_i(x_i)}\frac{\partial u_j}{\partial x_i}\right] \end{aligned} \tag{2}$$

2.2 Strong form of the PML in time domain

Applying the inverse Fourier transform to the system given above, the time strong form is written as:

$$\begin{aligned} \nabla.(\underline{\underline{\sigma}}\tilde{F}^e + \underline{\underline{\Sigma}}\tilde{F}^p) &= \rho f_m \ddot{\underline{u}} + \rho c_s f_c \dot{\underline{u}} + \mu f_k \underline{u} \\ \underline{\underline{\sigma}} &= C : \underline{\underline{\varepsilon}} \\ F^{eT}\dot{\underline{\underline{\epsilon}}}F^e + F^{pT}\underline{\underline{\varepsilon}}F^e + F^{eT}\underline{\underline{\varepsilon}}F^p + F^{pT}\underline{\underline{E}}F^p &= \frac{1}{2}(\nabla\dot{\underline{u}}^T F^e + F^{eT}\nabla\dot{\underline{u}}) + \frac{1}{2}(\nabla\underline{u}^T F^p + F^{pT}\nabla\underline{u}) \end{aligned} \tag{3}$$

with:

$$\begin{aligned} F^e &= \begin{bmatrix} 1+f_1^e(x_1) & 0 \\ 0 & 1+f_2^e(x_2) \end{bmatrix}, \quad F^p = \begin{bmatrix} c_s f_1^p(x_1) & 0 \\ 0 & c_s f_2^p(x_2) \end{bmatrix} \\ \tilde{F}^e &= \begin{bmatrix} 1+f_2^e(x_2) & 0 \\ 0 & 1+f_1^e(x_1) \end{bmatrix}, \quad \tilde{F}^p = \begin{bmatrix} c_s f_2^p(x_2) & 0 \\ 0 & c_s f_1^p(x_1) \end{bmatrix} \end{aligned} \tag{4}$$

and:

$$\begin{aligned} f_m : &= (1+f_1^e(x_1))\,(1+f_2^e(x_2)) \\ f_c : &= (1+f_1^e(x_1))\,f_2^p(x_2) + (1+f_2^e(x_2))\,f_1^p(x_1) \\ f_k : &= f_1^p(x_1)\,f_2^p(x_2) \end{aligned} \tag{5}$$

The tensors $\underline{\underline{\Sigma}}$ and $\underline{\underline{E}}$ are related to $\underline{\underline{\sigma}}$ and $\underline{\underline{\varepsilon}}$ by :

$$\underline{\underline{\Sigma}} = \int_{t=0}^{t} \underline{\underline{\sigma}}\, dt \qquad \underline{\underline{E}} = \int_{0}^{t} \underline{\underline{\varepsilon}}\, dt \tag{6}$$

In this work the damping function f_i^e, f_i^p will be linear as follow:

$$f_i^\alpha = a_\alpha \left(\frac{x_i - x_0}{d} \right)^n \qquad \alpha = e, p \qquad x_0 \leq x_i \leq x_0 + d \tag{7}$$

where a_α a positive integer.

Assuming a normal incidence and using the damping functions defined in Eq. (7), a_α can be expressed as a function of the reflection coefficient R by [13]:

$$a_\alpha = \frac{\frac{c_p}{c_s}(n+1)}{2d} \ln(\frac{1}{R}) \tag{8}$$

where c_p is the P wave velocity and c_s is the shear wave velocity.

2.3 Displacement based weak form of the PML

In this section, the discretization process proposed by Basu *et al* in [13] is presented. The space discretization is obtained using the finite element method while the time discretization is obtained using the classical Newmark schemes [15]. Let $\underline{v}$ be the test function belonging to an appropriate space, the weak formulation is obtained by integrating over the computational domain Ω:

$$\int_\Omega \rho f_m\, \underline{v}.\ddot{\underline{u}}\, d\Omega + \int_\Omega \rho\, c_s f_c \underline{v}.\dot{\underline{u}}\, d\Omega + \int_\Omega \mu\, f_k \underline{v}.\underline{u}\, d\Omega + \int_\Omega \underline{\underline{\tilde{\varepsilon}}}^e : \underline{\underline{\sigma}}\, d\Omega + \int_\Omega \underline{\underline{\tilde{\varepsilon}}}^p : \underline{\underline{\Sigma}}\, d\Omega = \int_\Gamma \underline{\omega}.(\underline{\underline{\sigma}}\tilde{F}^e + \underline{\underline{\Sigma}}\tilde{F}^p).\underline{n}\, d\Gamma \tag{9}$$

with $\Gamma = \partial\Omega$ the boundary of Ω, and $\underline{n}$ the normal vector to the Γ. $\underline{\underline{\tilde{\varepsilon}}}^e$ et $\underline{\underline{\tilde{\varepsilon}}}^p$ are given by:

$$\underline{\underline{\tilde{\varepsilon}}}^e = \frac{1}{2}(grad\underline{v}\, \tilde{F}^e + \tilde{F}^{eT}\, (grad\underline{v})^T) \qquad \underline{\underline{\tilde{\varepsilon}}}^p = \frac{1}{2}(grad\underline{v}\, \tilde{F}^p + \tilde{F}^{pT}\, (grad\underline{v})^T) \tag{10}$$

The mass, the damping and the stiffness matrices are given by:

$$m_{IJ} = \int_\Omega \rho f_m N_I N_J d\Omega\, I_d \quad c_{IJ} = \int_\Omega \rho f_c c_s N_I N_J d\Omega\, I_d \quad k_{IJ} = \int_\Omega \mu f_k N_I N_J d\Omega\, I_d \tag{11}$$

where N_I is the shape function of the node I. Taking into account the Eq. (9), the internal force term p_{n+1}^e is defined by:

$$p_{n+1}^e = \int_{\Omega_e} \tilde{B}^{eT} \hat{\sigma}_{n+1} + \int_{\Omega_e} \tilde{B}^{pT} \hat{\Sigma}_{n+1} \tag{12}$$

with $\tilde{B}^e$ and $\tilde{B}^p$ matrices depend on the shape functions and the damping functions given in terms of their nodal submatrices by:

$$\tilde{B}_I^e = \begin{bmatrix} \tilde{N}_{I1}^e & 0 \\ 0 & \tilde{N}_{I2}^e \\ \tilde{N}_{I2}^e & \tilde{N}_{I1}^e \end{bmatrix} \qquad \tilde{B}_I^p = \begin{bmatrix} \tilde{N}_{I1}^p & 0 \\ 0 & \tilde{N}_{I2}^p \\ \tilde{N}_{I2}^p & \tilde{N}_{I1}^p \end{bmatrix} \tag{13}$$

with:

$$\tilde{N}_{Ii}^e = \tilde{F}_{ji}^e N_{I,j} \quad et \quad \tilde{N}_{Ii}^p = \tilde{F}_{ji}^p N_{I,j} \tag{14}$$

The Voigt notation is adopted for the field $\hat{\sigma} = \begin{bmatrix} \sigma_{11} \\ \sigma_{22} \\ \sigma_{12} \end{bmatrix}$ and $\hat{\Sigma} = \begin{bmatrix} \Sigma_{11} \\ \Sigma_{22} \\ \Sigma_{12} \end{bmatrix}$ assumed to be linked according to the relationship:

$$\hat{\Sigma}_{n+1} = \hat{\Sigma}_n + dt\, \hat{\sigma}_{n+1} \tag{15}$$

It follows:

$$p_{n+1}^e = \int_{\Omega_e} \tilde{B}^T \hat{\sigma}_{n+1} + \int_{\Omega_e} \tilde{B}^{pT} \hat{\Sigma}_n \tag{16}$$

where:

$$\tilde{B}^T = \tilde{B}^{eT} + dt\, \tilde{B}^{pT} \tag{17}$$

The knowledge of $\hat{\sigma}_{n+1}$ depends on $\hat{\varepsilon}_{n+1}$ obtained by discretizing the 3^{rd} equation of the system (3) and assuming $\dot{\varepsilon}(t_{n+1}) = \frac{\varepsilon_{n+1} - \varepsilon_n}{dt}$ and $E(t_{n+1}) = E_n + dt\, \varepsilon_n$:

$$\hat{\varepsilon}_{n+1} = \frac{1}{dt} \left[B^{\varepsilon} \dot{U}_{n+1} + B^Q U_{n+1} + \frac{1}{dt} \hat{F}^{\varepsilon} \hat{\varepsilon}_n - \hat{F}^Q \hat{E}_n \right] \tag{18}$$

where B^{ε}, B^Q, $\hat{F}^{\varepsilon}$ and $\hat{F}^Q$ are matrices depending on the shape functions and the damping functions (see appendix A). The element interal force p_{n+1}^e can now be written in terms of the vectors v_{n+1} et u_{n+1} and the quantities at the time $t_n = ndt$. Finally, the weak form at the time t_{n+1} can be expressed as:

$$M\ddot{U}_{n+1} + (C + \widetilde{C})\dot{U}_{n+1} + (K + \widetilde{K})U_{n+1} + P(\varepsilon_n, E_n, \Sigma_n) = F_{ext} \tag{19}$$

P being an operator depending on the quatities at t_n.The global matrices $\widetilde{C}$, $\widetilde{K}$ are built using the following element submatrices:

$$\widetilde{c}^e = \frac{1}{dt} \int_{\Omega_e} \tilde{B}^T D B^{\varepsilon} \qquad \widetilde{k}^e = \frac{1}{dt} \int_{\Omega_e} \tilde{B}^T D B^Q \tag{20}$$

where D is given by:

$$D = \begin{bmatrix} \kappa + \frac{4}{3}\mu & \kappa - \frac{2}{3}\mu & 0 \\ \kappa - \frac{2}{3}\mu & \kappa + \frac{4}{3}\mu & . \\ 0 & 0 & \mu \end{bmatrix} \tag{21}$$

where μ is the shear modulus and κ is the bulk modulus. The last step involves the use of the Newmark schemes [15] and solves the problem in terms of displacement, velocity or acceleration.

3 Coupling algorithme physical domain and PML

Let Ω a bounded domain from $\mathbb{R}^2$ with a regular boundary. We assume that the domain Ω is divided into two parts Ω_1 and Ω_2 as illustrated in Figure 1 such as: $\Omega_1 \cap \Omega_2 = \oslash$ and $\partial\Omega_1 \cap \partial\Omega_2 = \Gamma^{12}$. Γ^{12} represents the interface between the two subdomains. The subdomain Ω_1 related to a non dissipative linear elastic behavior and the subdomain Ω_2 is related to a dissipative behavior characterized by the PML weak form given in Eq. (19).

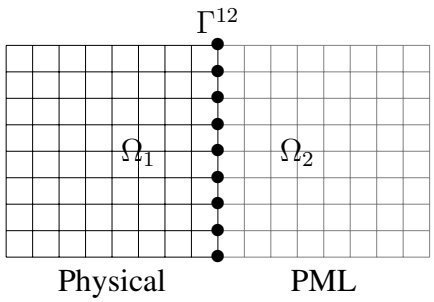

Figure 1: Domaine Ω partitionn en deux sous domaines Ω_1 et Ω_2

Subdomain Ω_1:

It is assumed that the medium Ω_1 is linear elastic characterized by the mass matrix M_1 and the stiffness matrix K_1. The semi-discrete in space equation of motion is given by:

$$M_1\ddot{U}_1 + K_1U_1 = F_{ext,1} - L_1^T\hat{\lambda} \tag{22}$$

where $\hat{\lambda}$ being the Lagrange multiplier vector corresponding to the nodal forces at the interface.

Subdomain Ω_2:

We assume that the subdomain 2 is governed by the discretized equation of motion in PML (19):

$$M_2\ddot{U}_2 + (C_2 + \widetilde{C}_2)\dot{U}_2 + (K_2 + \widetilde{K}_2)U_2 + P_2(\varepsilon_n, E_n, \Sigma_n) = -L_2^T\hat{\lambda} \tag{23}$$

L_1 and L_2 defined in Eq. (22) and Eq. (19) are boolean matrices, operating on nodal vectors associated with the two subdomains 1 and 2, and picks out the degrees of freedom lying on the interface Γ^{12} in order to ensure the velocity continuity at the interface, we write the following kinematic relationship:

$$L_1\dot{U}_1 + L_2\dot{U}_2 = 0 \tag{24}$$

In the following, the GC method [14] is employed to solve the previous problem. It is based on a dual Schur approach by introducing Lagrange multipliers $\hat{\lambda}$ to ensure the kinematic continuity at the interface. When discretizing in time the equation of motions for both subdomains, we have to choose the quantity (displacement, velocity or acceleration) whose continuity is imposed at the interface. Following the GC method, it has been proven by the authors that any Newmark time integrators can be coupled (for example, explicit central difference scheme

with implicit average acceleration scheme) when the continuity of velocities at the interface is prescribed. Thus, the constraint defined on velocities was adopted as written in Eq. (24).

Next the subdomain Ω_1 is integrated in time with an explicit time integration scheme (central difference scheme), characterized by the parameters $\gamma_1 = 0.5$ and $\beta_1 = 0$, whereas the subdomain Ω_2 is handled with an implicit time integration scheme (constant acceleration scheme), characterized by the parameters $\gamma_2 = 0.5$ and $\beta_2 = 0.25$. Note that main advantages of the coupling GC method is to provide heterogeneous time integration and multi-time step capabilities. The multi-time step capability is of great interest for minimizing the computation time required in the absorbing layer while keeping a target accuracy in the subdomain of interest. We focus on heterogeneous time integration of the coupled problem by using different time steps in the two subdomains. For this purpose, we define the fine time scale Δt_1 for the explicit domain and the coarse time scale Δt_2 for the implicit domain with $\Delta t_2 = m\Delta t_1$. The equation of motion is written for the subdomain 1 is prescribed at the time $t_m = \Delta t_2$ while the equation of motion of the subdomain 2 is prescribed at the time $t_j = j\Delta t_1$ $(j = 1, 2, ...m)$ as follows:

- Subdomain 1:

$$M_1\ddot{U}_1^j + K_1U_1^j = F_1^{ext,j} - L_1^T\hat{\lambda}^j \tag{25}$$

- Subdomain 2:

$$M_2\ddot{U}_2^m + (C_2 + \widetilde{C}_2)\dot{U}_2^m + (K_2 + \widetilde{K}_2)U_2^m + P_2(\varepsilon_0, E_0, \Sigma_0) = -L_2^T\hat{\lambda}^m \tag{26}$$

At the interface, the continuity of velocities is imposed at time t_j as:

$$L_1\dot{U}_1^j + L_2\dot{U}_2^j = 0 \tag{27}$$

From Newmark formula, we introduce the predictor quantities $U_1^{n-1,p}$ and $\dot{U}_1^{n-1,p}$ related to a time range $[t_n\,, t_{n+1}]$. They are determined from the quantities known at the beginning of time step as:

$$U_k^{n-1,p} = U_k^{n-1} + \Delta t\,\dot{U}_k^{n-1} + \Delta t^2\,(\frac{1}{2} - \beta_k)\,\ddot{U}_k^{n-1} \tag{28}$$

$$\dot{U}_k^{n-1,p} = \dot{U}_k^{n-1} + \Delta t\,(1 - \gamma_k)\,\ddot{U}_k^{n-1} \tag{29}$$

Using the expressions of the kinematic quantities in Eqs. (28) and (29), both equations of motion can be written in the form:

$$\widetilde{M_1}\ddot{U}_1^j = F_1^{ext,j} - K_1U_1^{j-1,p} - L_1^T\hat{\lambda}^j \tag{30}$$

$$\widetilde{M_2}\ddot{U}_2^m = -P_2(\varepsilon_0, E_0, \Sigma_0) - (C_2 + \widetilde{C}_2)\dot{U}_2^{0,p} - (K_2 + \widetilde{K}_2)U_2^{0,p} - L_2^T\hat{\lambda}^m \tag{31}$$

with the effective stiffness matrices defined for both subdomains by:

$$\widetilde{M_1} = M_1 + \beta_1\Delta t_1^2K_1 \tag{32}$$

$$\widetilde{M_2} = M_2 + \beta_2\Delta t_2^2(K_2 + \widetilde{K}_2) + \gamma_2\Delta t(C_2 + \widetilde{C}_2) \tag{33}$$

The procedure proposed by Gravouil and Combescure is based on splitting the kinematic quantities into two parts: the free and the linked quantities. The free quantities are obtained by only considering the internal and external forces, whereas the linked quantities are obtained by taking into account only the interface loads defined by the Lagrange multiplier vector $\hat{\lambda}$. For example, if we consider the subdomain Ω_2, the discrete equation of motion is split into two parts as follows:

$$\begin{cases} \widetilde{M}_2 \ddot{U}_2^{free,m} = -P_2(\varepsilon_0, E_0, \Sigma_0) - (C_2 + \widetilde{C}_2)\dot{U}_2^{0,p} - (K_2 + \widetilde{K}_2)U_2^{0,p} \\ \widetilde{M}_2 \ddot{U}_2^{link,m} = -L_2^T \hat{\lambda}^m \end{cases} \tag{34}$$

The complete accelerations are obtained by summing the two parts as: $\ddot{U}_2^m = \ddot{U}_2^{free,m} + \ddot{U}_2^{link,m}$.

The same procedure is applied to the subdomain Ω_1 at each time t_j. Furthermore, the kinematic quantities of the subdomain 2 at t_j are interpolated as well as the Lagrange multiplier :

$$\begin{cases} \hat{\lambda}^j = (1 - \frac{j}{m})\hat{\lambda}^0 + \frac{j}{m}\hat{\lambda}^m \\ W_2^j = (1 - \frac{j}{m})W_2^0 + \frac{j}{m}W_2^m \end{cases} \tag{35}$$

Where W_2^j denote the free or the linked velocities of the subdomain 2 at t_j. Using the kinematic condition at the interface in Eq. (27) at each time t_j, we obtain:

$$L_1 \dot{U}_1^{link,j} + L_2 \dot{U}_2^{link,j} = -L_1 \dot{U}_1^{free,j} - L_2 \dot{U}_2^{free,j} \tag{36}$$

Then, by using Eq. (35) and the expression of the velocities as a function of accelerations, the following interface problem can be derived:

$$H\hat{\lambda}^j = b_j \tag{37}$$

with the interface operator and the second side member vector defined by:

$$\begin{cases} H = \gamma_1 \Delta t L_1 \widetilde{M}_1^{-1} L_1^T + \gamma_2 \Delta t L_2 \widetilde{M}_2^{-1} L_2^T \\ b_j = L_1 \dot{U}_1^{free,j} + L_2 \dot{U}_2^{free,j} \end{cases} \tag{38}$$

Finally, once we get the values of the Lagrange multiplier vector at the end time of the time step, linked accelerations are obtained and thus complete accelerations as well as displacements and velocities from Newmark formula in Eqs. (28) and (29).

4 Numerical examples

In the following numerical applications, non harmonic waves will be investigated by considering a Ricker incident wave Ric defined by:

$$Ric\,(t,\, t_p,\, t_s) = A\,(2\,\pi^2\,\frac{(t-t_s)^2}{t_p^2} -\, 1)\,\exp(-\pi^2 \frac{(t-t_s)^2}{t_p^2}) \tag{39}$$

The Ricker wave is characterized by three parameters: the fundamental period t_p, the time shift t_s and the amplitude A. The chosen values are: $t_p = 3s$, $t_s = 3s$ and $A = 0.1$, as illustrated in Figure 2.

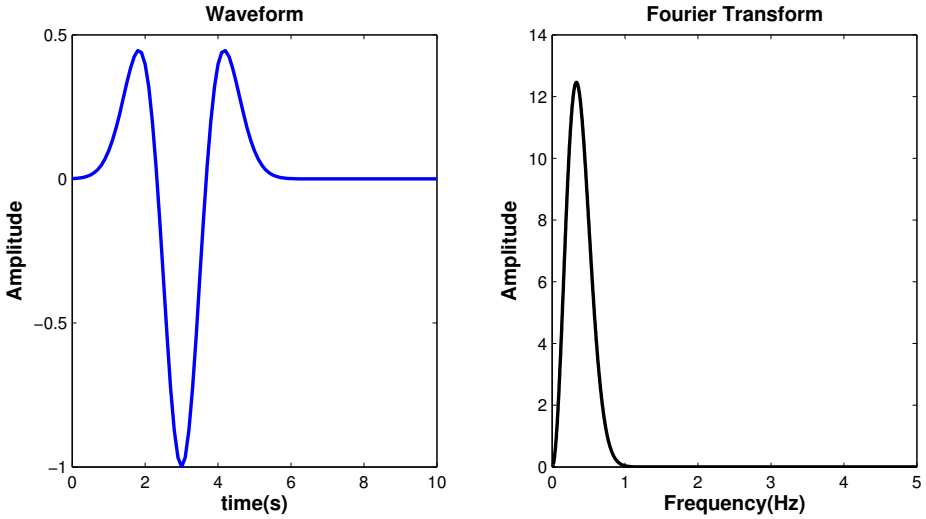

Figure 2: Waveform and Fourier transform of the Ricker wavelet

4.1 Lamb Test

Lamb's test consists in applying a concentrated load, characterized by the Ricker form in our study, to the surface of a ground assumed to be infinite in both directions. A sensor is located at a distance d from the load point in order to record the vertical and the horizontal displacements at this point. In 1904 Lamb [19] analytically calculated the displacements at a given point of the surface by assuming an isotropic linear elastic behavior for the soil. The derived theoretical solution exhibits the complexity of the problem since there are many types of waves traveling through the soil (P and S-waves, Rayleigh waves, etc).

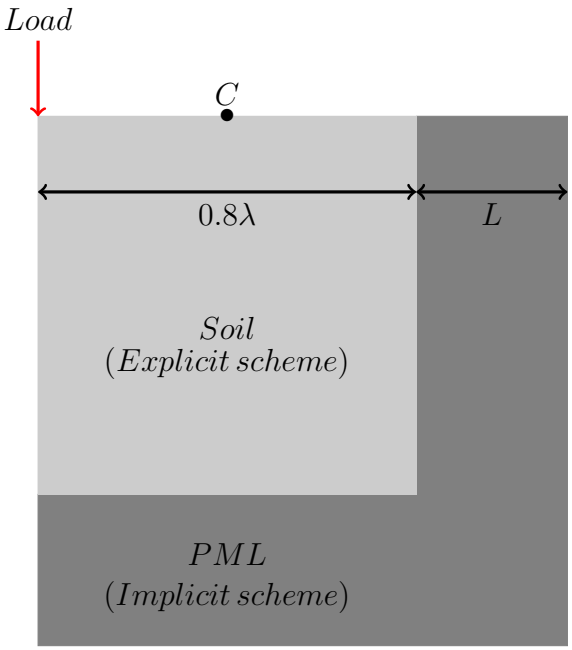

Figure 3: Modeling Lamb test using PMLs. The soil is integrated using explicit time scheme while the PML is integrated using implicit time scheme.

The Lamb test is modeled using the bounded-domain-PML as illustrated in Figure 3, com-

posed of a bounded soil (subdomain 1) with a size of 0.8λ and a PML (subdomain 2) characterized by a thickness L, The bounded problem is descritized using the four-node bilinear isoparametric elements. The soil is supposed to be linear elastic with ρ_1, $E_1 = 1$ and $\nu_1 = 0.24$. The attenuation functions are chosen as $f_i^e = 0$ and $f_i^p = a_p \left(\frac{x_i - x_0}{L}\right)$ with $a_p = 10$ and $x_0 = 4$. The length $L = 2$ is calculated using the following value of the reflection coefficient $R = 0.001$ and the relationship in Eq. (8). Finally, a point C located at the distance of 2 from the load point is chosen in order to record the vertical and the horizontal displacements.

In this part, the numerical solution is computed using the multi time step GC method. Two computations are distinguished: the first called Explicit/Explicit computation deals with the case where the both subdomains are intergrated with the explicit scheme and the second called Explicit/Implicit computation deals with the case where the subdomain 1 is integrated with the explicit scheme and the subdomain 2 is integrated with the implicit scheme. Next, the purpose is to analyze the effect of varying the ratio m on the accuracy of the results given in terms of displacements at the point C and energies in the physical domain (soil).

Before going further, we start by estimating the error introduced by the PML model with respect to the initial problem with an unbounded domain. For this purpose, we define the relative error due to the PML model and related to the quantity E over the time range $[0, T]$ by $err = \frac{\|E_{PML} - E_{ref}\|_{L^2([0,T])}}{\|E_{ref}\|_{L^2([0,T])}}$, where E_{PML} is the value of E obtained using the PML and E_{ref} is the value of E obtained using an extended mesh. In both cases, the computation is dealt with an explicit scheme. Figures 4 and 5 compare the displacements and energies obtained using the PML model with results obtained using an extended mesh. Note the excellent agreement between the results since the error, defined above, does not exceed 1% for the displacements and 0.1% for the energies.

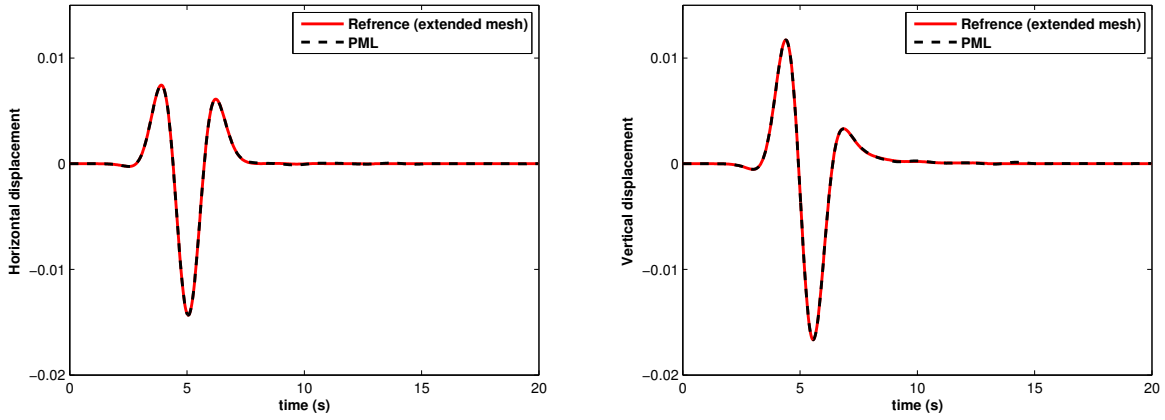

(a) Horizontal displacement

(b) Vertical displacement

Figure 4: Vertical and horizontal displacements plotted at point C using time homogeneous explicit PMLs compared to the reference results using an extended mesh.

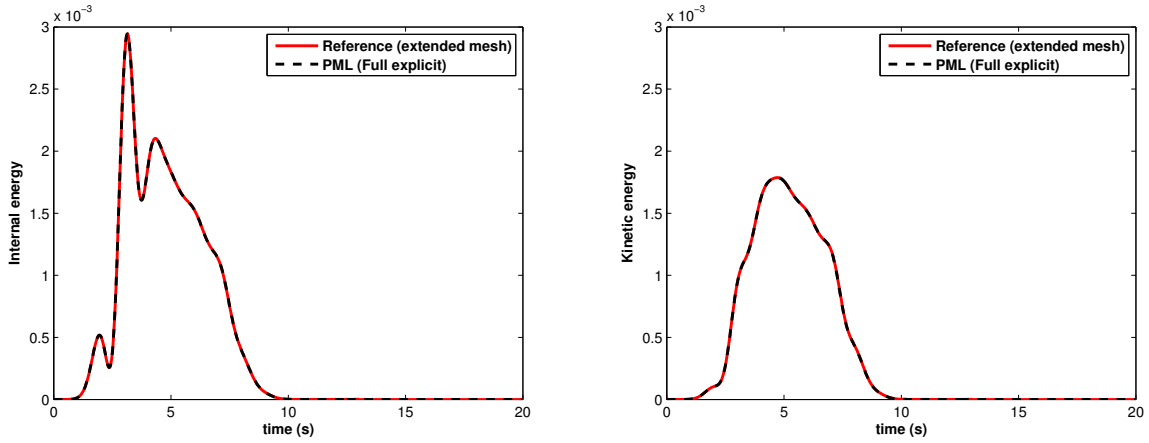

(a) Energie potentielle (b) Energie cintique

Figure 5: Kinetic and internal energies computed using time homogeneous explicit PMLs compared to the reference results using an extended mesh.

The error due to the coupling strategy Explicit/Implicit over the time range $[0, T]$ is defined by $err = \frac{\|E_{I/E}^{(m)} - E_{ref}\|_{L^2([0,T])}}{\|E_{ref}\|_{L^2([0,T])}}$, where $E_{I/E}^{(m)}$ is the value of E obtained using the GC method with the ratio m and E_{ref} is the value of E obtained using a full explicit computation. Figures 6 and 7 compare the results obtained using the Explicit/Implicit computation with different values of m with the results obtained using the Explicit/Explicit computation. One can remark that the different quantities (displacements and energies) are in a good agreement even if small fluctuations can be observed in the case of $m = 5$. Table 1 summarizes the errors computed for each quantity by varying the ratio m from 1 to 5. It can be observed that the errors are globally small and does not exceed 3.6% for the displacements and 0.7% for the energies.

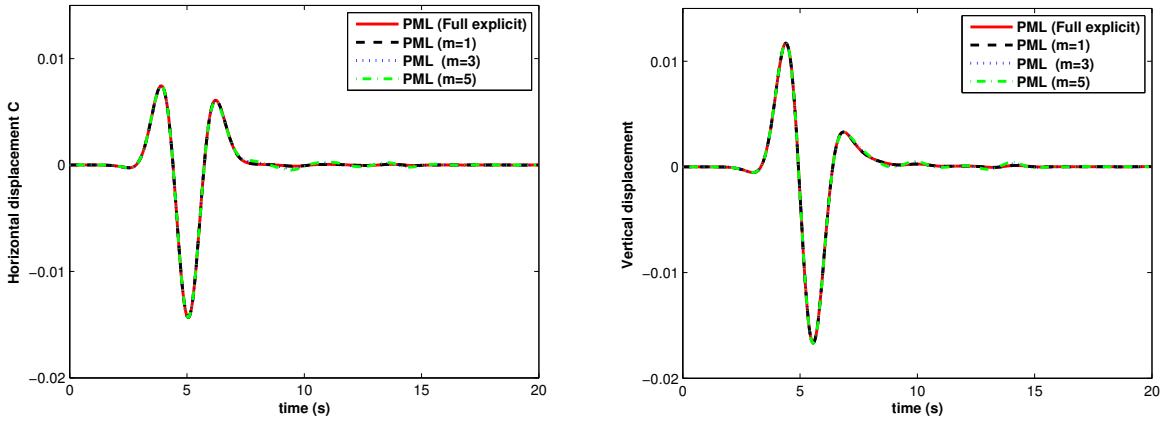

(a) Horizontal displacement (b) Vertical displacement

Figure 6: Vertical and horizontal displacements plotted at point C using time heterogeneous implicit PMLs for different values of the tiem step ratio m compared to the reference results using a full explicit integration.

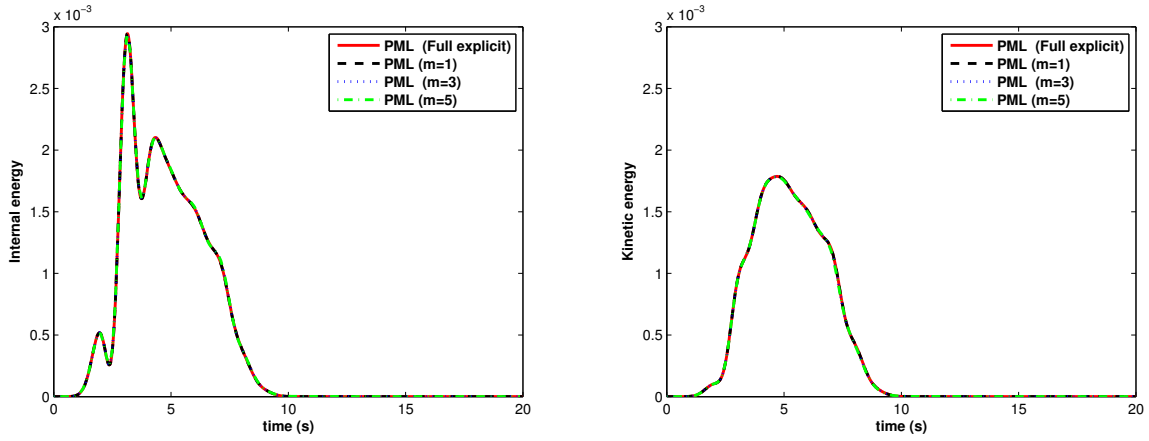

(a) Energie potentielle

(b) Energie cintique

Figure 7: Kinetic and internal energies computed using time heterogeneous implicit PMLs for different values of time step ratio m compared to the reference results using a full explicit integration.

	Kinetic energy	Internal energy	Horizontal displacement	Vertical displacement
$m = 1$	0.0002%	0.003%	0.001%	0.001%
$m = 3$	0.3%	0.1%	1.8%	1.3%
$m = 5$	0.7%	0.3%	3.6%	2.6%

Table 1: Relative errors related to the kinetic and internal energies computed for PMLs for different time step ratios m.

4.2 Rigid strip on a homogeneous isotropic elastic half-plane

In Figure 8, the classical problem of the rigid strip-footing (strip Young's modulus very important with respect to the soil Young's modulus) on a half plane is considered. The study is very similar to the previous one except that the strip will play the role of the third subdomain integrated with the implicit scheme. Using the GC method, the system composed of the PML and the strip will be integrated with the same time step computed from the soil properties instead of the strip properties which will be very small due to the stiffness of the strip.

We keep the same properties of the soil and the PML given in the previous Lamb test. The cross section is characterized by a half width 0.5 and a Young's modulus 100 times that of the soil. The load is varying as a Ricker wave with the parameters defined before and is applied uniformly to the strip as it is shown in Figure 8. The comparison will be in terms of displacements computed at the point C and energies by considering the system composed of the strip and the soil.

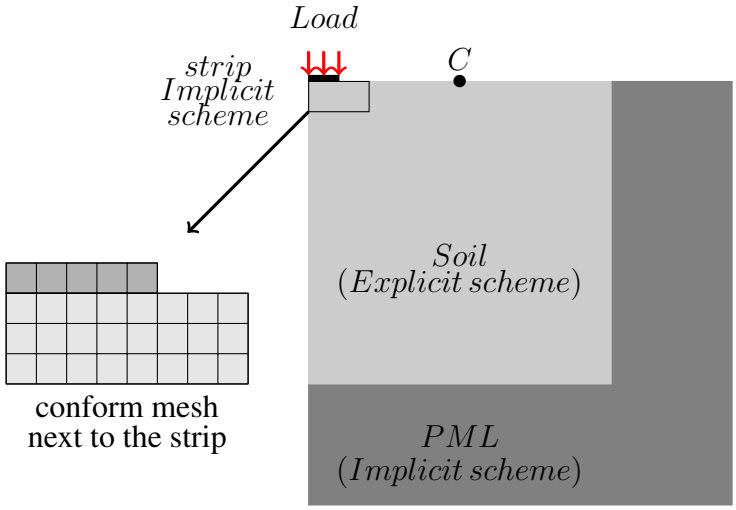

Figure 8: Rigid strip on a homogeneous soil. The soil and the strip are integrated using explicit time scheme while the PML is integrated using implicit time scheme.

Figure 9 compares the displacements at C obtained using the PML model and the extended mesh (reference results). It can be observed that the results closely match the reference results with an error, estimated using the definition in the previous example, less than 2%.

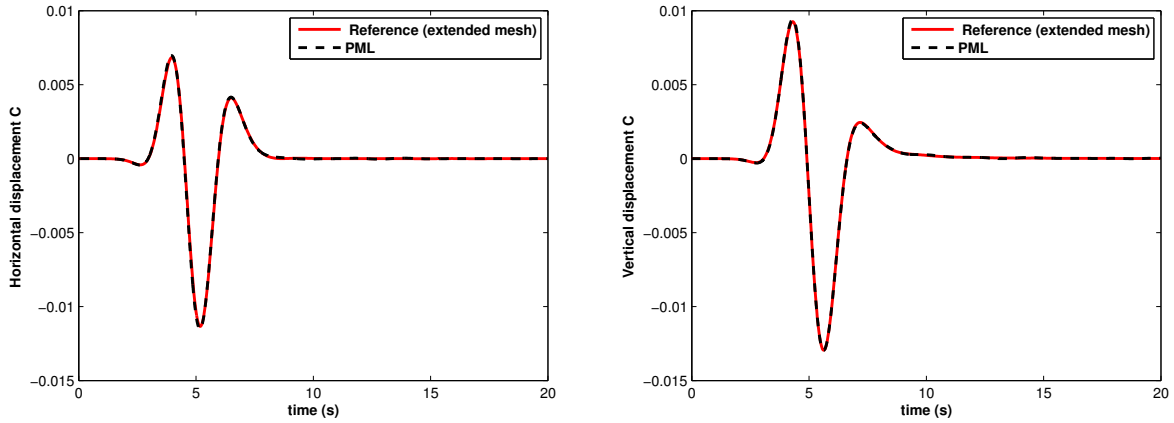

(a) Horizontal displacement

(b) Vertical displacement

Figure 9: Vertical and horizontal displacements plotted at point C using the PMLs compared to the reference results using an extended mesh.

Considering the subdomain decomposition described before, Figures 10 and 11 compare the displacements and the energies obtained using the Explicit/Implicit strategy by varying the time ratio m with the results obtained using a full explicit integration. It can be noted that the different curves are quite close with an error less than 5% for the displacements and 2.4% for the energies (Table 2). Furthermore, an important reduction in time computation has been observed which is on the order of 6,16 and 21 times less than the full explicit computation for $m = 1$, $m = 3$ and $m = 5$ respectively.

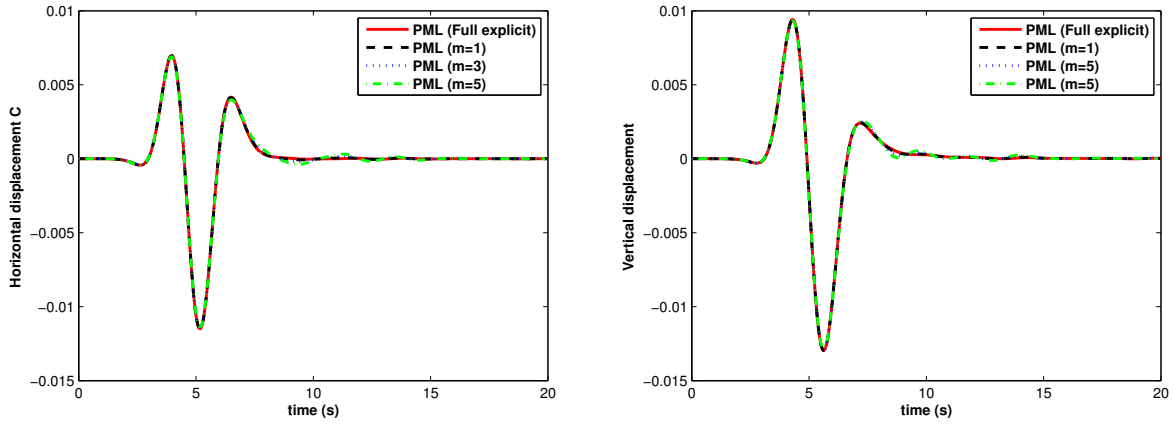

(a) Horizontal displacement (b) Vertical displacement

Figure 10: Vertical and horizontal displacements plotted at point C using time heterogeneous implicit PMLs for different values of time step ratios m compared the reference results using a full explicit integration.

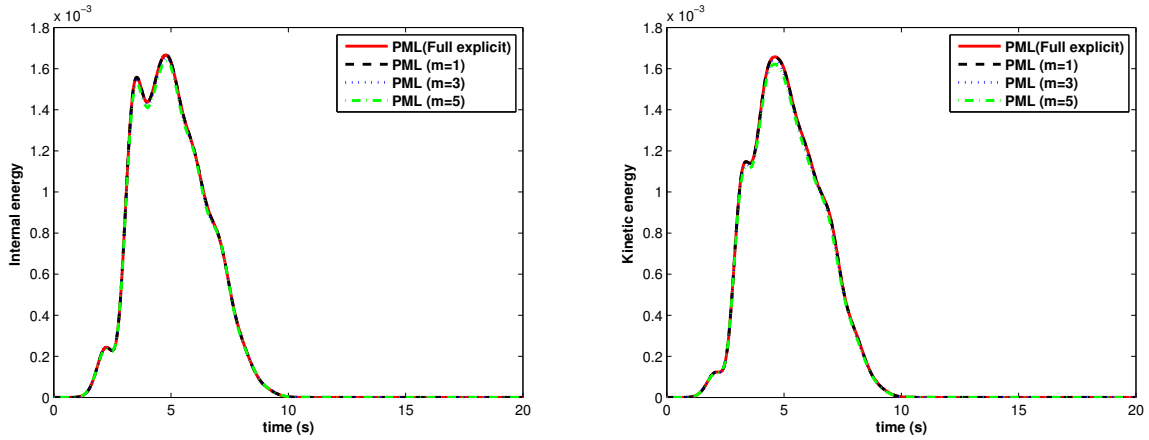

(a) Energie potentielle (b) Energie cintique

Figure 11: Kinetic and internal energies computed using time heterogeneous implicit PMLs for different values of time step ratios m compared to the reference results using a full explicit integration.

	Kinetic energy	Internal energy	Horizontal displacement	Vertical displacement
$m = 1$	0.2%	0.1%	0.8%	0.6%
$m = 3$	1.3%	0.9%	3%	2%
$m = 5$	2.4%	1.8%	5%	3.7%

Table 2: Relative errors related to the kinetic and internal energies computed for the system composed of the strip and the soil by varying the time step ratios m from 1 to 5.

5 Conclusion

In this paper, we presented the multi−time step coupling algorithm, based on GC method, between the PML developed by Basu *et al* in [13] and a physical domain assumed to be linear isotropic. The resulting algorithm was tested numerically through the computation of displacements and energies for two 2D applications. These tests indicate that the proposed coupling strategy offers interesting results in terms of accuracy and CPU time. However, a sensitivity to a relatively small values of the time ratio m was observed for both tests, maybe due the numerical dissipation introduced by the GC method. The extension of this method to other coupling strategies (Brun *et al* [20] for example) is in progress.

Anppendix A

The matrices B^{ϵ},B^{Q}, $\hat{F}^{\epsilon}$ and $\hat{F}^{Q}$ in equation 18 are defined by:
First, we give the following definitions:

$$F^{l} = \left[F^{p} + \frac{F^{e}}{dt}\right]^{-1} \qquad F^{\epsilon} = F^{e}F^{l} \quad F^{Q} = F^{p}F^{l} \tag{40}$$

The matrix B^{ϵ} is given in term of the submatrix for the node I by:

$$B^{\epsilon}_{I} = \begin{bmatrix} F^{\epsilon}_{11}N^{l}_{I1} & F^{\epsilon}_{21}N^{l}_{I1} \\ F^{\epsilon}_{12}N^{l}_{I2} & F^{\epsilon}_{22}N^{l}_{I2} \\ F^{\epsilon}_{11}N^{l}_{I2} + F^{\epsilon}_{12}N^{l}_{I1} & F^{\epsilon}_{21}N^{l}_{I12} + F^{\epsilon}_{22}N^{l}_{I1} \end{bmatrix} \tag{41}$$

with:

$$N^{l}_{Ii} = F^{l}_{ij}N_{I,j} \tag{42}$$

The matrix B^{Q} is defined, similarly, by replacing F^{ϵ} with F^{Q}. Finally, the matrix $\hat{F}^{\epsilon}$ is given by:

$$\hat{F}^{\epsilon} = \begin{bmatrix} (F^{\epsilon}_{11})^{2} & (F^{\epsilon}_{21})^{2} & F^{\epsilon}_{11}F^{\epsilon}_{21} \\ (F^{\epsilon}_{12})^{2} & (F^{\epsilon}_{22})^{2} & F^{\epsilon}_{12}F^{\epsilon}_{22} \\ 2F^{\epsilon}_{11}F^{\epsilon}_{12} & 2F^{\epsilon}_{21}F^{\epsilon}_{22} & F^{\epsilon}_{11}F^{\epsilon}_{22} + F^{\epsilon}_{12}F^{\epsilon}_{21} \end{bmatrix} \tag{43}$$

likewise, the matrix $\hat{F}^{Q}$ is obtained by replacing F^{ϵ} with F^{Q}.

References

[1] P. Bettess. Infinite elements. *International Journal for Numerical Methods in Engineering*, 11:53–64, 1977.

[2] B. Enquist and A. Majda. Absorbing boundary conditions for the numerical simulation of waves. *Mathematics of Computation*, 31:629–65, 1977.

[3] J. F. Semblat, L. Lenti, and A. Gandomzadeh. A simple multi-directional absorbing layer method to simulate elastic wave propagation in unbounded domains. *International Journal for Numerical Methods in Engineering*, 85:1543–1563, 2011.

[4] P. Rajagopal, M. Drozdz, E. A. Skelton, M.J. S. Lowe, and R. V. Craster. On the use of the absorbing layers to simulate the propagation of elastic waves in unbounded isotropic media using commercially available finite element packages. *NDT&E International*, 51:30–40, 2012.

[5] E. Zafati, M. Brun, I. Djeran-Maigre, and F. Prunier. Multi-directional and multi-time step absorbing layer for unbounded domain. *Comptes Rendus Mecanique*, 342:539–557, 2014.

[6] W.C. Chew and Q.H. Liu. Perfectly matched layers for elastodynamics: a new absorbing boundary condition. *Journal of Computational Acoustics*, 4:341–359, 1996.

[7] J. Bérenger. A perfectly matched layer for the absorption of electromagnetic waves. *Journal of Computational Physics*, 114:185–200, 1994.

[8] F. Hastings, J.B. Schneider, and S.L. Broschat. Application of the perfectly matched layer (pml) absorbing boundary condition to elastic wave propagation. *The Journal of the Acoustical Society of America*, 100:3061–3069, 1996.

[9] F. Collino and C. Tsoga. Application of the perfectly matched layer model to the linear elastodynamic problem in anisotropic heterogeneous media. *Geophysics*, 66:294–307, 2001.

[10] T. Wang and X. Tang. Finite-difference modeling of elastic wave propagation: a nonsplitting perfectly matched approach. *Geophysics*, 68:1749–1755, 2003.

[11] R. Matzen. An efficient finite element time-domain formulation for the elastic second-order wave equation: A non split complex frequency shifted convolutional pml. *International Journal for Numerical Methods in Engineering*, 88:951–973, 2011.

[12] U. Basu and A.K. Chopra. Perfectly matched layers for time-harmonic elastodynamics of unbounded domains: theory and finite-element implementation. *International Journal for Numerical Methods in Engineering*, 192:1337–1375, 2003.

[13] U. Basu and A.K. Chopra. Perfectly matched layers for transient elastodynamics of unbouded domains. *International Journal for Numerical Methods in Engineering*, 59:1039–1074, 2004.

[14] A. Combescure and A. Gravouil. A numerical scheme to couple subdomains with different time-steps for predominantly linear transient analysis. *Computer Methods in Applied Mechanics and Engineering*, 191:1129–1157, 2002.

[15] N.M. Newmark. A method of computation for structural dynamics. *Journal of the Engineering Mechanics Division (ASCE)*, 85:67–94, 1959.

[16] T.J.R. Hughes. *The Finite Element Method: Linear Static and Dynamic Finite Element Analysis*. Prentice-Hall, Englewood Cliffs, NJ, 1987.

[17] N. Mahjoubi, A. Gravouil, and A. Combescure. Coupling subdomains with heterogeneous time integrators and incompatible time steps. *Computational Mechanics*, pages DOI 10.1007/s00466–009–0413–4, 2009.

[18] U. Basu. Explicit finite element perfectly matched layer for transient three-dimensional elastic waves. *International Journal for Numerical Methods in Engineering*, 77:151–176, 2009.

[19] H. Lamb. On the propagation of tremors over the surface of an elastic solid. *Proceeedings of the Royal Society of London*, 72:128–130, 1903.

[20] M. Brun, A. Gravouil, A. Combescure, and A. Limam. Two FETI-besed heterogeneous time step coupling methods for Newmark and α-schemes derived from the energy method. *Computer methods in applied mechanics and engineering*, 283:130–176, 2015.